Targeting mitochondrial oxidative phosphorylation eradicates therapy-resistant chronic myeloid leukaemic stem cells

Elodie M. Kuntz[1], Pablo Baquero[2], Alison M. Michie[3], Karen Dunn[3], Saverio Tardito[1], Tessa L. Holyoake[3], G. Vignir Helgason[2,5] & Eyal Gottlieb[1,4,5]

[1]Cancer Research UK, Beatson Institute, Garscube Estate, Switchback Road, Glasgow G61 1BD, UK. [2]Wolfson Wohl Cancer Research Centre, Institute of Cancer Sciences, College of Medical, Veterinary & Life Sciences, University of Glasgow, G61 1QH, UK. [3]Paul O'Gorman Leukaemia Research Centre, Institute of Cancer Sciences, College of Medical, Veterinary & Life Sciences, University of Glasgow, Glasgow, G12 0ZD, UK. [4]Technion Integrated Cancer Center, Faculty of Medicine, Technion - Israel Institute of Technology, Haifa, 3525433, Israel. [5]These authors jointly directed this work. Correspondence should be addressed to G.V.H. (Vignir.Helgason@Glasgow.ac.uk) and E.G. (e.gottlieb@technion.ac.il)

Treatment of chronic myeloid leukaemia (CML) with imatinib mesylate and other second/third generation c-Abl specific tyrosine kinase inhibitors (TKIs) has significantly extended patient survival[1]. However, TKIs primarily target differentiated cells and do not eliminate leukaemic stem cells (LSCs)[2-4]. Therefore, targeting minimal residual disease (MRD), to prevent acquired resistance and/or disease relapse requires identification of novel LSC-selective target(s) that can be exploited therapeutically[5,6]. Given that malignant transformation involves cellular metabolic changes, which may in turn render the transformed cells susceptible to specific assaults in a selective manner[7], we searched for such vulnerabilities in CML LSCs. We performed metabolic analyses on both stem cell-enriched ($CD34^+$ and $CD34^+CD38^-$) and differentiated ($CD34^-$) patient derived CML cells, and compared their signature with that of normal counterparts. Combining stable isotope-assisted metabolomics with functional assays, we demonstrate that primitive CML cells rely on upregulated oxidative metabolism for their survival. We also show that combination-treatment of imatinib with tigecycline, an antibiotic that inhibits mitochondrial protein translation, selectively eradicates CML LSCs, both *in vitro* and in a xenotransplantation model of human CML. Our findings provide a strong indication for investigating the employment of TKIs in combination with tigecycline to treat CML patients with MRD.

CML is a myeloproliferative disorder brought about by the chromosomal translocation t(9;22)(q34;q11) in a haemopoietic stem cell (HSC)[8,9] that drives the expansion of a leukaemic clone via BCR-ABL expression, a chimeric onco-protein with a constitutive tyrosine kinase activity[10]. Prolonged treatment with TKIs carries risks of drug toxicity and/or acquired resistance, and entails high economic costs to sustain remission. On the other hand, rapid relapse in half of the patients is seen after treatment discontinuation[11-13]. Therefore, to obtain potential curative treatments that effectively eradicate CML LSCs, we specifically studied patient-derived stem cell-enriched $CD34^+$ CML cells. In culture, proliferating untreated $CD34^+$ primary CML cells rapidly lose surface CD34 expression (**Supplementary Fig. 1a**). Imatinib treatment primarily targets differentiated $CD34^-$ CML cells for apoptosis, leading to enrichment of more primitive $CD34^+$ cells (**Supplementary Fig. 1a**,**b**). Consequently, imatinib decreases the efficiency of primary CML progenitor cells to form colonies in a short term colony forming cell (CFC) assay but, in line with the resistance of CML stem cells to TKI treatment, it does not affect the colony forming capacity of $CD34^+$ cell in a long-term culture-initiating cell (LTC-IC) assay (**Supplementary Fig. 1c,d**).

Since stem cells can exhibit different metabolic traits compared to their corresponding differentiated cells[14-16], we metabolically profiled $CD34^+$ and $CD34^-$ CML cells derived from four patients by recording the steady-state levels of 70 metabolites central to glucose, nucleotide, amino acid, fatty acid and energy metabolism, through liquid chromatography-mass spectrometry (LC-MS). The pattern of metabolites in stem cell-enriched population compared to differentiated CML cells revealed a potential increase in lipolysis and fatty acid oxidation; we found an increase in glycerol-3-phosphate, carnitine and acylcarnitine derivatives, as well as a decrease in free fatty acids, such as oleic and stearic acids (**Fig. 1a** and **Supplementary Table 1**). Of note, fatty acid oxidation has been associated with the

maintenance of HSCs and potentially with leukaemogenesis[17,18]. In order to validate and further substantiate these findings, leukaemic cells were cultured for 24 hours in the presence of uniformly $^{13}C_{16}$-labelled palmitate, and ^{13}C isotopic enrichment in different palmitate-derived metabolites was measured by LC-MS. Substantial enhancement in palmitate-derived carbon in tricarboxylic acid (TCA) cycle metabolites and TCA cycle-derived amino acids was recognised in $CD34^+$ leukaemic cells in comparison to the differentiated $CD34^-$ cells of the same patient (**Supplementary Fig. 2a**). Furthermore, the steady state levels of these metabolites were increased in stem cell-enriched CML populations, while lactate levels were decreased (**Fig. 1a**, **Supplementary Fig. 2a** and **Table 1**). The steady state levels of aspartate was recently recognised as *bona-fide* indicators of mitochondrial oxidative capacity[19-21]. Accordingly, CML cells derived from four patients presented on average a 3.0-fold increase in mitochondrial oxygen consumption rates in $CD34^+$ cells compared to patient-matched $CD34^-$ cells. Moreover, the complete decrease in oxygen consumption upon ATP synthase inhibition with oligomycin demonstrated that the increased oxygen consumption is tightly linked to ATP production in these cells (**Fig. 1b**,**c**). However, the increase in the steady state levels of TCA cycle metabolites and the derived amino acids could not be solely explained by an increase in fatty acid oxidation, as the production of acetyl coenzyme A (CoA) from palmitate does not support a net production of TCA cycle metabolites (anaplerosis).

To study oxidative metabolism and anaplerosis in more detail, glucose, an anaplerosis enabling metabolite, was traced in leukaemic cells cultured for 24 hours with uniformly $^{13}C_6$-labelled glucose. This revealed that in $CD34^+$ CML cells, TCA cycle metabolites contained a significantly larger fraction of isotopologues with 2, 3 or more ^{13}C atoms compared to those in $CD34^-$ cells (**Fig. 1d**). The larger fractions of labelled TCA cycle-derived glutamate and aspartate observed in $CD34^+$ CML cells confirmed their higher oxidative and anaplerotic

activity. Concurrently, $CD34^+$ cells demonstrated a noticeable (although not significant) decrease in glucose-derived lactate ($^{13}C_3$-lactate) indicating that pyruvate is indeed more effectively shunted towards the TCA cycle (**Fig. 1d**). Increased acetyl CoA levels produced from fatty acid oxidation are predicted to increase the anaplerotic activity of pyruvate carboxylase (PC), but potentially to inhibit pyruvate dehydrogenase (PDH) activity. We therefore estimated the relative metabolic contribution of both enzymes in $^{13}C_6$-glucose-labelled $CD34^+$ compared to $CD34^-$ CML cells by assessing the isotopic distribution of the nearest detected relevant product ($^{13}C_3$-aspartate for PC and $^{13}C_2$-citrate for PDH). While no change in PDH activity was detected between the two CML cell subsets, the relative activity of PC was significantly higher in $CD34^+$ CML cells, further confirming their increased oxidative anaplerotic metabolism (**Supplementary Fig. 2b,c)**.

To investigate whether this oxidative phenotype is unique to primitive CML cells, we assessed the metabolic profile of $CD34^+$ cells from four CML patients and compared with normal haemopoietic $CD34^+$ cells from four donors. Higher steady state levels of carnitine and acylcarnitine derivatives and lower levels of free fatty acids, such as oleic and linolenic acids, were detected in $CD34^+$ CML cells (**Supplementary Fig. 3a and Supplementary Table 2**). In line with this, the ^{13}C enrichment of citrate, glutamate and aspartate from $^{13}C_{16}$-palmitate was significantly higher in $CD34^+$ CML cells in comparison to $CD34^+$ normal cells, demonstrating that the increase in fatty acid oxidation observed previously is selective to $CD34^+$ CML cells (**Supplementary Fig. 3b-d**). Following incubation with $^{13}C_6$-glucose, the enrichment of glucose-derived ^{13}C isotopes in citrate, glutamate and aspartate was significantly higher in $CD34^+$ CML cells compared to their normal counterparts which, combined with a significant increase in both PC and PDH relative activity, demonstrated a selective increase in glucose oxidation and anaplerosis in the leukaemic cells (**Fig. 2a-c,**

Supplementary Fig. 3e,f). Moreover, the mitochondrial respiration of leukaemic $CD34^+$ samples was on average 3.3-fold higher than that of $CD34^+$ normal cells (**Fig. 2d,e**). As $CD34^+$ cell pools contain both stem and progenitor cells, we next verified our findings in a $CD34^+CD38^-$ CML cell population; a rare quiescent sub-population (~5% of total $CD34^+$) that is further enriched for LSCs. Flow cytometry analysis of mitochondrial content and mitochondrial membrane potential suggested that CML LSCs possess increased mitochondrial oxidative functions compared to normal HSCs (**Fig. 2f-i**). Moreover, $^{13}C_6$-glucose incubation of $CD34^+CD38^-$ cells isolated from two CML patients revealed that $CD34^+CD38^-$ CML cells contained increased levels of ^{13}C isotopologues for citrate, aspartate and glutamate compared to $CD34^+CD38^-$ normal cells, confirming that CML LSCs have an increased oxidative metabolism (**Fig. 2j-l and Supplementary Fig. 3g-i**).

These findings suggest that in primitive CML cells, mitochondrial oxidative metabolism is crucial for production of energy and anabolic precursors and that restraining their mitochondrial functions may have a therapeutic benefit. Tigecycline is an FDA-approved antibiotic, which inhibits bacterial protein synthesis. Due to the similarity between mitochondrial and bacterial ribosomes, it also inhibits the synthesis of mitochondria-encoded proteins, all of which are required for the oxidative phosphorylation machinery[22]. Previous reports demonstrated therapeutic efficacy of tigecycline against cancer cells, including primary acute myeloid leukaemic cells[23] and the oxidative subtype of diffuse large B-cell lymphoma[22]. First, we demonstrated that tigecycline is capable of inhibiting the translation of the mitochondrial-encoded proteins MT-CO1 and MT-CO2, but not the nuclear-encoded mitochondrial proteins ATP5A or UQCRC2 (**Fig. 3a** and **Supplementary Fig. 4a**). This was associated with a compensatory increase in MT-CO1 and MT-CO2 mRNA levels (**Supplementary Fig. 4b**). In line with this, tigecycline treatment significantly impaired

mitochondrial respiration of $CD34^+$ CML cells (**Supplementary Fig. 4c**). Primary $CD34^+$ CML cells were then cultured with $^{13}C_6$-glucose for 24 hours in the absence or presence of tigecycline. A robust and significant decrease in glucose oxidation was noted in tigecycline-treated cells, with a 2.8-3.4-fold decrease in the incorporation of ^{13}C isotopes into citrate, glutamate and aspartate (**Fig. 3b-d**). Tigecycline had a broad effect on cellular metabolism as illustrated by a combined decrease in respiration and extracellular acidification rate (**Supplementary Fig. 4c,d**) indicative of a concurrent impairment of oxidative phosphorylation and glycolysis. This was associated with a decrease in both PDH and PC relative activity (**Supplementary Fig. 4e,f)**. Similarly, $CD34^+$ CML cells treated with tigecycline displayed a significant decrease in the fraction of isotopologues with 2 or more ^{13}C atoms following incubation with $^{13}C_5$-glutamine and $^{13}C_{16}$-palmitate (**Supplementary Fig. 4g-l**). In tandem to blocking oxidative metabolism, tigecycline treatment decreased the overall steady-state levels of aspartate (**Fig. 3d**), in support of the anaplerotic role of oxidative metabolism in the LSCs-enriched population.

Oxidative phosphorylation and anaplerosis are essential for growth and proliferation. Labelling of $CD34^+$ CML cells with a fluorescent cell division tracker revealed that tigecycline alone, or in combination with imatinib, strongly impaired proliferation of primary $CD34^+$ CML cells, whereas imatinib alone had only a moderate effect, in line with its preferential effect on differentiated $CD34^-$ cells (**Fig. 3e**). Furthermore, treatment with imatinib or tigecycline alone decreased the number of short-term CML CFC, with their combined application effectively eliminating colony formation (**Fig. 3f,g).** This effect on colony growth correlated with an increase in cell death, measured by Annexin V staining (**Supplementary Fig. 5a,b**). Importantly, neither drug, alone or in combination, had a significant effect on normal, non-leukaemic CFCs, affirming a potential therapeutic window (**Fig. 3h**). Thus far, our studies

suggest that the combined inhibitory effect of tigecycline and imatinib on CFCs may result from the effect of the drugs on two distinct populations, where imatinib targets more mature progenitors, while tigecycline targets the more oxidative, long-term LSCs. To test this hypothesis, LTC-IC assay was performed: $CD34^+$ CML cells were treated once with imatinib or tigecycline, alone or in combination, followed by liquid culture for 5 weeks prior to placing them in semi-solid medium. This ensures selective measurements of the functional capacity of long-term LSCs, since short-term progenitor cells lose their colony forming potential during the 5 weeks culture. This stringent *in vitro* stem cell assay revealed that while imatinib was ineffective, tigecycline-mediated inhibition of oxidative metabolism significantly decreased CML LSC potential (**Fig. 3i**). Similar findings were observed when the mitochondrial complex I inhibitor phenformin was used (**Supplementary Fig. 5c,d**).

To further assess the clinical relevance of these findings, we moved to a robust xenotransplantation model of human CML. Sub-lethally irradiated immuno-compromised mice were transplanted with $CD34^+$ human CML cells. Six weeks later, engraftment was assessed by recording the percentage of cells expressing human leukocyte common antigen ($CD45^+$) from the total peripheral leukocytes in the blood (**Fig. 4a**). After ensuring equivalent and sufficient engraftment of human cells in all mice (**Supplementary Fig. 6a**), mice were treated daily from 6 weeks post-transplantation for a period of 4 weeks with vehicle only, tigecycline (escalating doses of 25-100 $mg.kg^{-1}$: see Methods), imatinib (100 $mg.kg^{-1}$) or both drugs combined (**Fig. 4a**). In all experimental arms, no changes in body or spleen weight or signs of toxicity were observed during treatment and total bone marrow cellularity was unaffected, confirming excellent tolerability (**Supplementary Fig. 6b-d**). Importantly, the decreased level of mitochondria-encoded proteins was used as a pharmacodynamic biomarker to demonstrate on-target action of tigecycline *in vivo* (**Supplementary Fig. 6e**). Following

treatment, bone marrow cells were extracted and analysed by flow cytometry for the expression of the human antigens CD45 (leukocytes), CD34 (progenitors and stem cells) and CD38 (to distinguish between $CD34^+CD38^+$ progenitors and $CD34^+CD38^-$ LSCs). The majority of bone marrow cells were non-leukaemic host cells (human $CD45^-$) and, as indicated above, were unaffected by the treatment (**Fig. 4b** and **Supplementary Fig. 7a**). In contrast, the total number of CML-derived $CD45^+$ cells in the bone marrow was decreased, though marginally, in tigecycline treated mice and significantly in mice treated with imatinib (**Supplementary Fig. 7b**). Importantly, in the combination arm, the CML burden was further decreased, and when only undifferentiated bone marrow $CD45^+CD34^+$ CML cells were analysed, these results were even more pronounced (**Fig. 4b,c** and **Supplementary Fig. 7a,b**). The most striking effect though was seen within the more primitive human LSCs population. Whereas imatinib alone only marginally (and insignificantly) decreased the number of $CD45^+CD34^+CD38^-$ CML cells, the combination treatment eliminated 95% of these cells (**Fig. 4d**).

Experiments using cord blood $CD34^+$ cells showed that both imatinib and tigecycline, either alone or in combination, had a marginal effect on engrafted normal blood cells (**Supplementary Figure 8a-c**). Finally, an additional two cohorts of mice were transplanted with $CD34^+$ CML cells and treated as before. To investigate whether the combination of tigecycline and imatinib slowed the rate of relapse, both cohorts were then left untreated for an additional two (experiment 1) or three (experiment 2) weeks. Bone marrow analysis following drug withdrawal demonstrated that while mice treated with imatinib as a single agent showed signs of relapse (with the number of leukaemic cells similar to untreated mice), the vast majority of mice treated with the combination of tigecycline and imatinib sustained low numbers of LSCs in the bone marrow (**Fig. 4e,f**).

Taken together, our findings indicate that primitive CML stem/progenitor cells are highly susceptible to the inhibition of oxidative phosphorylation, while $CD34^+$ normal cells are not. This previously unknown metabolic vulnerability shown here represents a therapeutic target for treatment with the FDA-approved mitochondrial translation inhibitor tigecycline. Finally, *in vivo*, combining tigecycline treatment with the standard-of-care drug, imatinib, produces a selective cytotoxic effect on $CD34^+$ CML and on more primitive LSCs at clinically administrable doses.

ACKNOWLEDGEMENTS

We thank all patients and healthy donors who contributed samples; A. Hair for sample processing; T. Gilbey and T. Harvey for cell sorting; N. Van Den Broek and G. MacKay for technical assistance and A. King for editorial work. This study was supported by Cancer Research UK; the Cancer Research UK Glasgow Centre (C596/A18076) and the BSU facilities at the Cancer Research UK Beatson Institute (C596/A17196); MRC/AstraZeneca project grants (MR/K014854/1); the Glasgow Experimental Cancer Medicine Centre (ECMC), which is funded by Cancer Research UK and by the Chief Scientist's Office (Scotland); the Howat Foundation and Friends of Paul O'Gorman; Bloodwise Specialist Programme (14033); the Kay Kendall Leukaemia Fund (KKL501 and KKL698); Lady Tata International Award; Leuka. G.V.H. is a KKLF Intermediate Research Fellow/Leadership Fellow/John Goldman Fellow.

AUTHORS CONTRIBUTION

E.M.K., G.V.H. and E.G. wrote the manuscript. E.M.K., P.B., T.L.H., G.V.H. and E.G. designed experiments and interpreted data. E.M.K. and P.B. performed experiments and

analysed data. A.M.M. and K.D. assisted with the *in vivo* work. S.T. provided the custom-formulated culture medium. T.L.H. and G.V.H. provided primary cells. G.V.H. and E.G. supervised the project. All authors reviewed the manuscript.

COMPETING FINANCIAL INTERESTS

E.G. is a Founder and Shareholder of MetaboMed Ltd. T.L.H. has previously received research support from Bristol-Myers Squibb and Novartis

REFERENCES

1. Druker, B.J., *et al.* Five-year follow-up of patients receiving imatinib for chronic myeloid leukemia. *N Engl J Med* **355**, 2408-2417 (2006).
2. Graham, S.M., *et al.* Primitive, quiescent, Philadelphia-positive stem cells from patients with chronic myeloid leukemia are insensitive to STI571 in vitro. *Blood* **99**, 319-325 (2002).
3. Corbin, A.S., *et al.* Human chronic myeloid leukemia stem cells are insensitive to imatinib despite inhibition of BCR-ABL activity. *J Clin Invest* **121**, 396-409 (2011).
4. Hamilton, A., *et al.* Chronic myeloid leukemia stem cells are not dependent on Bcr-Abl kinase activity for their survival. *Blood* **119**, 1501-1510 (2012).
5. Holyoake, T.L. & Helgason, G.V. Do we need more drugs for chronic myeloid leukemia? *Immunological reviews* **263**, 106-123 (2015).
6. Abraham, S.A., *et al.* Dual targeting of p53 and c-MYC selectively eliminates leukaemic stem cells. *Nature* **534**, 341-346 (2016).
7. Tennant, D.A., Duran, R.V. & Gottlieb, E. Targeting metabolic transformation for cancer therapy. *Nature reviews. Cancer* **10**, 267-277 (2010).
8. Rowley, J.D. Letter: A new consistent chromosomal abnormality in chronic myelogenous leukaemia identified by quinacrine fluorescence and Giemsa staining. *Nature* **243**, 290-293 (1973).
9. Groffen, J., *et al.* Philadelphia chromosomal breakpoints are clustered within a limited region, bcr, on chromosome 22. *Cell* **36**, 93-99 (1984).
10. Konopka, J.B., Watanabe, S.M. & Witte, O.N. An alteration of the human c-abl protein in K562 leukemia cells unmasks associated tyrosine kinase activity. *Cell* **37**, 1035-1042 (1984).
11. Rousselot, P., *et al.* Imatinib mesylate discontinuation in patients with chronic myelogenous leukemia in complete molecular remission for more than 2 years. *Blood* **109**, 58-60 (2007).
12. Mahon, F.X., *et al.* Discontinuation of imatinib in patients with chronic myeloid leukaemia who have maintained complete molecular remission for at least 2 years: the prospective, multicentre Stop Imatinib (STIM) trial. *Lancet Oncol* **11**, 1029-1035 (2010).
13. Ross, D.M., *et al.* Safety and efficacy of imatinib cessation for CML patients with stable undetectable minimal residual disease: results from the TWISTER study. *Blood* **122**, 515-522 (2013).
14. Simsek, T., *et al.* The distinct metabolic profile of hematopoietic stem cells reflects their location in a hypoxic niche. *Cell stem cell* **7**, 380-390 (2010).

15. Takubo, K., *et al.* Regulation of glycolysis by Pdk functions as a metabolic checkpoint for cell cycle quiescence in hematopoietic stem cells. *Cell stem cell* **12**, 49-61 (2013).
16. Yu, W.M., *et al.* Metabolic regulation by the mitochondrial phosphatase PTPMT1 is required for hematopoietic stem cell differentiation. *Cell stem cell* **12**, 62-74 (2013).
17. Ito, K., *et al.* A PML-PPAR-delta pathway for fatty acid oxidation regulates hematopoietic stem cell maintenance. *Nat Med* **18**, 1350-1358 (2012).
18. Carracedo, A., Cantley, L.C. & Pandolfi, P.P. Cancer metabolism: fatty acid oxidation in the limelight. *Nature reviews. Cancer* **13**, 227-232 (2013).
19. Sullivan, L.B., *et al.* Supporting Aspartate Biosynthesis Is an Essential Function of Respiration in Proliferating Cells. *Cell* **162**, 552-563 (2015).
20. Birsoy, K., *et al.* An Essential Role of the Mitochondrial Electron Transport Chain in Cell Proliferation Is to Enable Aspartate Synthesis. *Cell* **162**, 540-551 (2015).
21. Cardaci, S., *et al.* Pyruvate carboxylation enables growth of SDH-deficient cells by supporting aspartate biosynthesis. *Nat Cell Biol* **17**, 1317-1326 (2015).
22. Norberg, E., *et al.* Differential contribution of the mitochondrial translation pathway to the survival of diffuse large B-cell lymphoma subsets. *Cell Death Differ* (2016).
23. Skrtic, M., *et al.* Inhibition of mitochondrial translation as a therapeutic strategy for human acute myeloid leukemia. *Cancer Cell* **20**, 674-688 (2011).

FIGURE LEGENDS

Figure 1 Primitive CML cells show an increase in oxidative metabolism compared to differentiated counterparts. (**a**) Comparative steady-state metabolomics analysis of patient-matched $CD34^+$ and $CD34^-$ CML cells measured by LC-MS. Mean, n=4 patients. (**b**) Representative respirometry output in $CD34^+$ and $CD34^-$ CML cells. Mean ± S.D. (**c**) Basal mitochondrial oxygen consumption rate (OCR) of $CD34^+$ and $CD34^-$ CML cells. Mean ± S.E.M. n=4 patient samples. (**d**) Relative isotopologue distribution of indicated metabolites in $CD34^+$ and $CD34^-$ CML cells measured by LC-MS following 24 hours incubation with $^{13}C_6$-labelled glucose. Acetyl-CoA could not be detected by LC-MS in our experimental conditions. Mean ± S.E.M. n=3 patient samples. FC, fold change of glucose-derived ($^{13}C \geq 2$) metabolite abundance relative to $CD34^-$ CML cells. PDH, Pyruvate dehydrogenase; PC, Pyruvate carboxylase. P values were calculated with paired Student's t-test.

Figure 2 Enhanced mitochondrial metabolic activity in primitive CML cells compared to normal undifferentiated haemopoietic cells. (**a-c**) Relative isotopologue distribution of (**a**) citrate, (**b**) glutamate and (**c**) aspartate in $CD34^+$ CML and $CD34^+$ normal cells measured by LC-MS following 24 hours incubation with $^{13}C_6$-labelled glucose. Mean ± S.E.M. n=5 patient and normal samples. FC, Fold change of glucose-derived ($^{13}C \geq 2$) metabolite abundance relative to CD34+ normal cells. P values were calculated by unpaired Student's t-test. (**d**) Representative respirometry output in $CD34^+$ CML and $CD34^+$ normal cells. Mean ± S.D. (**e**) Basal mitochondrial OCR. Mean ± S.E.M. n=9 patient samples and n=4 normal samples. P values were calculated by unpaired Student's t-test. (**f**) Representative histograms of Mitotracker Green-labelled $CD34^+CD38^-$ CML cells (blue) and $CD34^+CD38^-$ normal cells

(red). (**g**) Mitochondrial content of $CD34^+CD38^-$ CML cells and $CD34^+CD38^-$ normal cells was determined from the geometric mean of Mitotracker Green-labelled cells. Mean ± S.E.M. n=3 patient and 3 normal samples. P values were determined by one sample t-test. (**h**) Representative histograms of TMRM-labelled $CD34^+CD38^-$ CML (blue) and $CD34^+CD38^-$ normal (red) cells. (**i**) Mitochondrial membrane potential of $CD34^+CD38^-$ CML cells and $CD34^+CD38^-$ normal cells was determined from the geometric mean of TMRM-labelled cells. Mean ± S.E.M. n=3 patient and 3 normal samples. FC, fold change relative to normal cells. P values were determined by one sample t-test. (**j-l**) Relative isotopologue distribution of (**j**) citrate, (**k**) glutamate and (**l**) aspartate in $CD34^+CD38^-$ CML and $CD34^+CD38^-$ normal cells measured by LC-MS following 24 hours incubation with $^{13}C_6$-labelled glucose. n=1 patient sample.

Figure 3 Inhibition of aberrant oxidative metabolism targets CML progenitors and LSCs**.** (**a**) Protein expression in $CD34^+$ CML cells following a 72 hours *in vitro* treatment with tigecycline (2.5 µM). n=1 patient sample. (**b-d**) Relative isotopologue distribution of (**b**) citrate, (**c**) glutamate and (**d**) aspartate in $CD34^+$ CML cells measured by LC-MS following 24 hours incubation with $^{13}C_6$-labelled glucose in the presence or absence of tigecycline (2.5 µM). Mean ± S.E.M. n=3 patient samples. (**e**) Representative flow cytometry histograms obtained from cellular division tracking of CellTrace Violet-stained $CD34^+$ CML cells following 72 hours treatment with vehicle only, tigecycline (2.5 µM), imatinib (2 µM) and combination (2.5 µM + 2 µM). (**f**) Representative images of colonies and (**g**) colony numbers following 3 days drug treatment of $CD34^+$ CML cells. Mean ± S.E.M. n=4 patient samples. (**h**) Colony number of $CD34^+$ normal cells following 72 hours drug treatment with the indicated drugs. Mean ± S.E.M. n=4 normal samples. (**i**) Number of colonies measured by LTC-IC assay in $CD34^+$ CML cells.

Mean ± S.E.M. n=5 patient samples. FC, Fold change of glucose-derived ($^{13}C \geq 2$) metabolite abundance relative to tigecycline-treated $CD34^+$ CML cells. TIG, tigecycline; IM, imatinib; Combo, combination. P values were calculated by paired Student's t-test.

Figure 4 Inhibition of oxidative metabolism eliminates xenotransplanted human CML LSCs. (**a**) Diagram of experimental design. The pre-treatment engraftment levels of CML cells in mice were assessed by monitoring the percentage of human $CD45^+$ circulating leukocytes using flow cytometry. (**b**) Representative analyses of human CD45 and CD34 expression in murine bone marrow was used to assess engrafted CML cells following the indicated treatment. (**c**) Number of human $CD34^+$ and (**d**) human $CD34^+CD38^-$ CML cells remaining in the bone marrow following *in vivo* drug treatment. (**e**) Number of human $CD34^+$ and (**f**) human $CD34^+CD38^-$ CML cells remaining in the bone marrow following 2 (experiment 1) or 3 (experiment 2) weeks of drug discontinuation. n≥5 mice per treatment arm. TIG, tigecycline; IM, imatinib. P values were calculated by unpaired Student's t-test on logarithmic transformed variables to meet the assumption of normality.

Figure 1

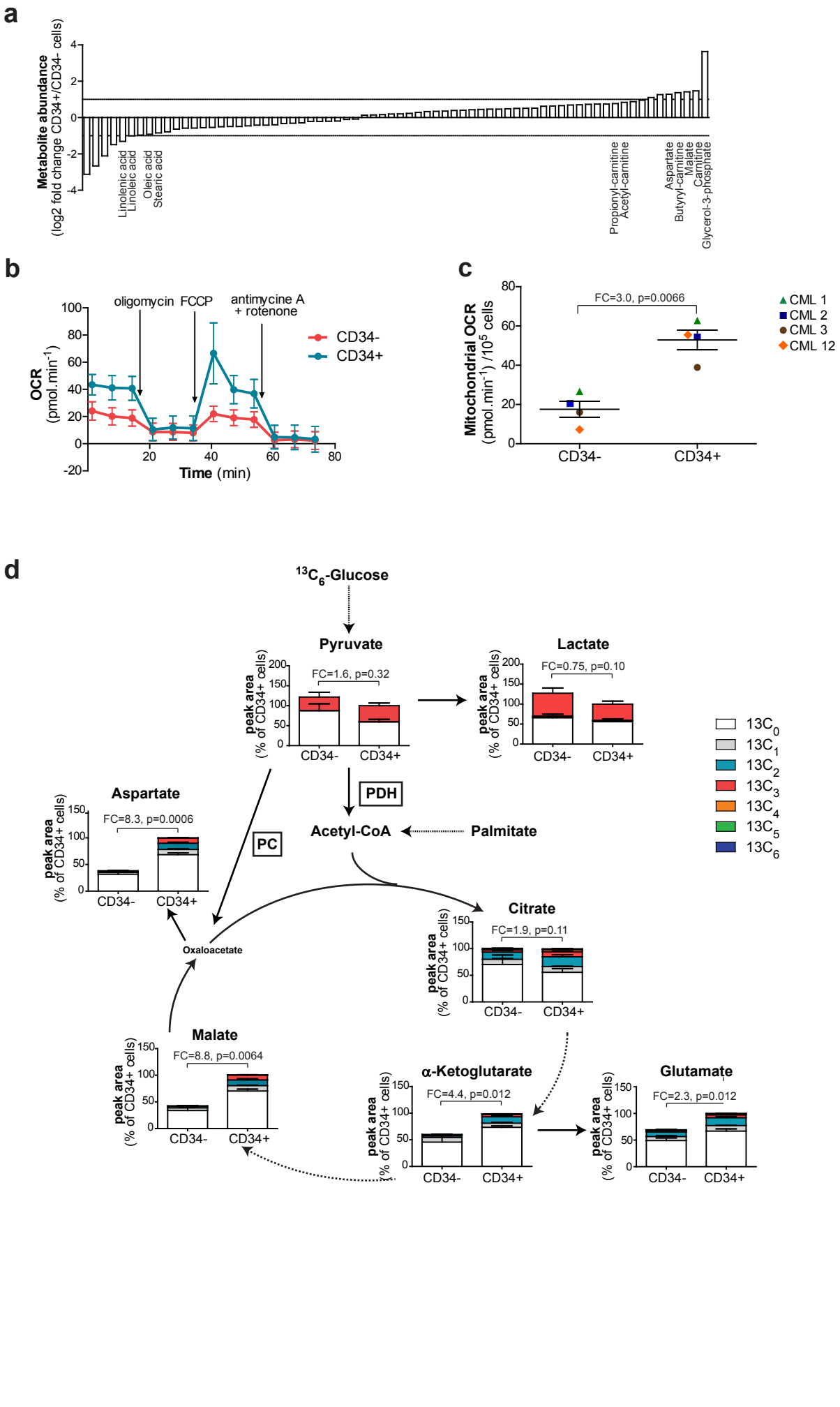
a
Metabolite abundance
(log2 fold change CD34+/CD34- cells)
Linolenic acid
Linoleic acid
Oleic acid
Stearic acid
Propionyl-carnitine
Acetyl-carnitine
Aspartate
Butyryl-carnitine
Malate
Carnitine
Glycerol-3-phosphate
b
oligomycin
FCCP
antimycine A
+ rotenone
CD34-
CD34+
OCR
(pmol.min-1)
Time (min)
c
FC=3.0, p=0.0066
Mitochondrial OCR
(pmol.min-1) /10^5 cells
CML 1
CML 2
CML 3
CML 12
d
13C6-Glucose
Pyruvate
FC=1.6, p=0.32
Lactate
FC=0.75, p=0.10
PDH
PC
Acetyl-CoA
Palmitate
Aspartate
FC=8.3, p=0.0006
Oxaloacetate
Citrate
FC=1.9, p=0.11
Malate
FC=8.8, p=0.0064
α-Ketoglutarate
FC=4.4, p=0.012
Glutamate
FC=2.3, p=0.012
peak area
(% of CD34+ cells)
13C0
13C1
13C2
13C3
13C4
13C5
13C6

Figure 2

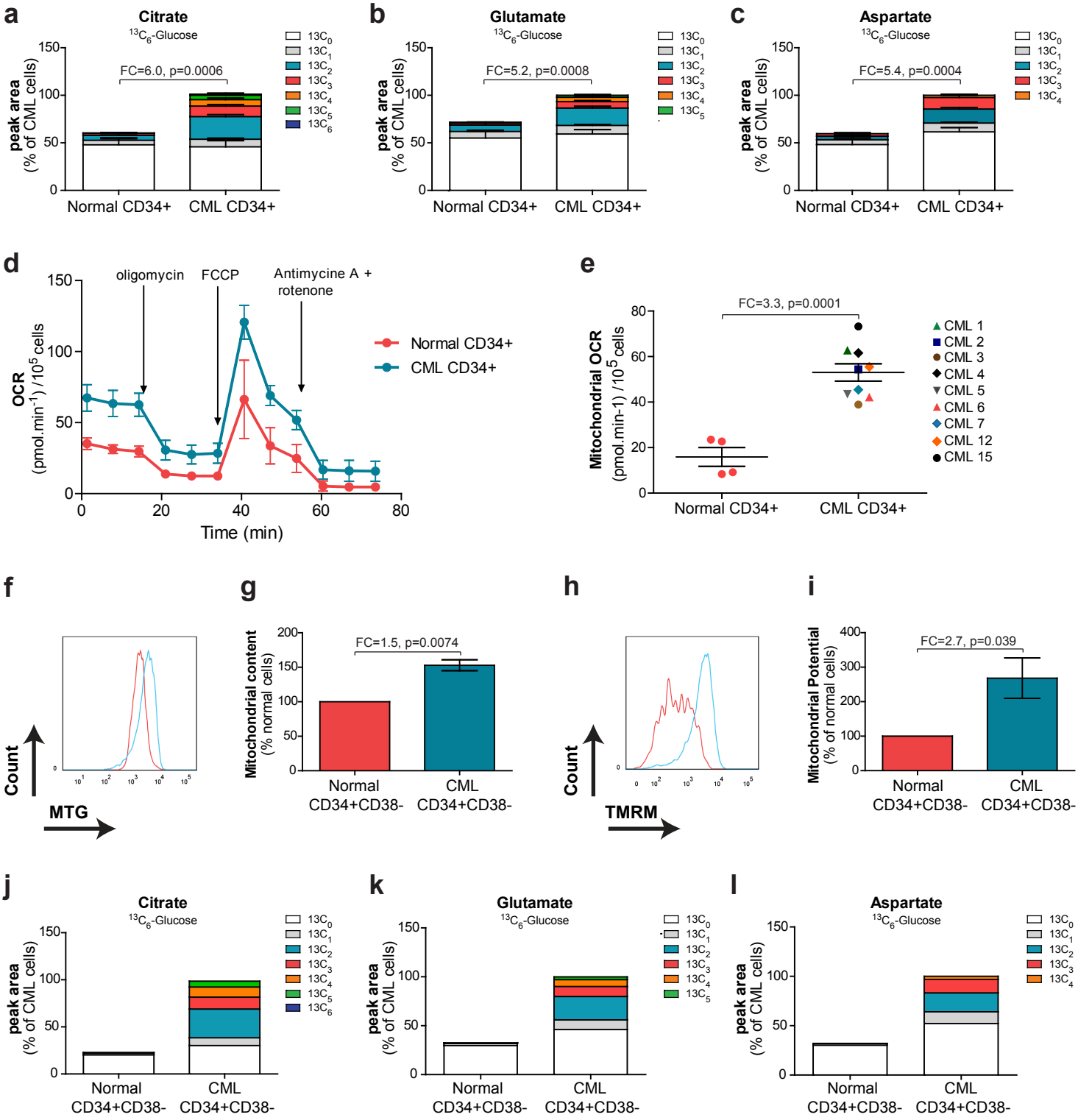
a
Citrate
$^{13}C_6$-Glucose
peak area (% of CML cells)
FC=6.0, p=0.0006
Normal CD34+
CML CD34+
$^{13}C_0$
$^{13}C_1$
$^{13}C_2$
$^{13}C_3$
$^{13}C_4$
$^{13}C_5$
$^{13}C_6$
b
Glutamate
$^{13}C_6$-Glucose
peak area (% of CML cells)
FC=5.2, p=0.0008
Normal CD34+
CML CD34+
c
Aspartate
$^{13}C_6$-Glucose
peak area (% of CML cells)
FC=5.4, p=0.0004
Normal CD34+
CML CD34+
d
OCR (pmol.min^{-1}) /10^5 cells
oligomycin
FCCP
Antimycine A + rotenone
Normal CD34+
CML CD34+
Time (min)
e
Mitochondrial OCR (pmol.min-1) /10^5 cells
FC=3.3, p=0.0001
Normal CD34+
CML CD34+
CML 1
CML 2
CML 3
CML 4
CML 5
CML 6
CML 7
CML 12
CML 15
f
Count
MTG
g
Mitochondrial content (% normal cells)
FC=1.5, p=0.0074
Normal CD34+CD38-
CML CD34+CD38-
h
Count
TMRM
i
Mitochondrial Potential (% of normal cells)
FC=2.7, p=0.039
Normal CD34+CD38-
CML CD34+CD38-
j
Citrate
$^{13}C_6$-Glucose
peak area (% of CML cells)
Normal CD34+CD38-
CML CD34+CD38-
k
Glutamate
$^{13}C_6$-Glucose
peak area (% of CML cells)
Normal CD34+CD38-
CML CD34+CD38-
l
Aspartate
$^{13}C_6$-Glucose
peak area (% of CML cells)
Normal CD34+CD38-
CML CD34+CD38-

Figure 3

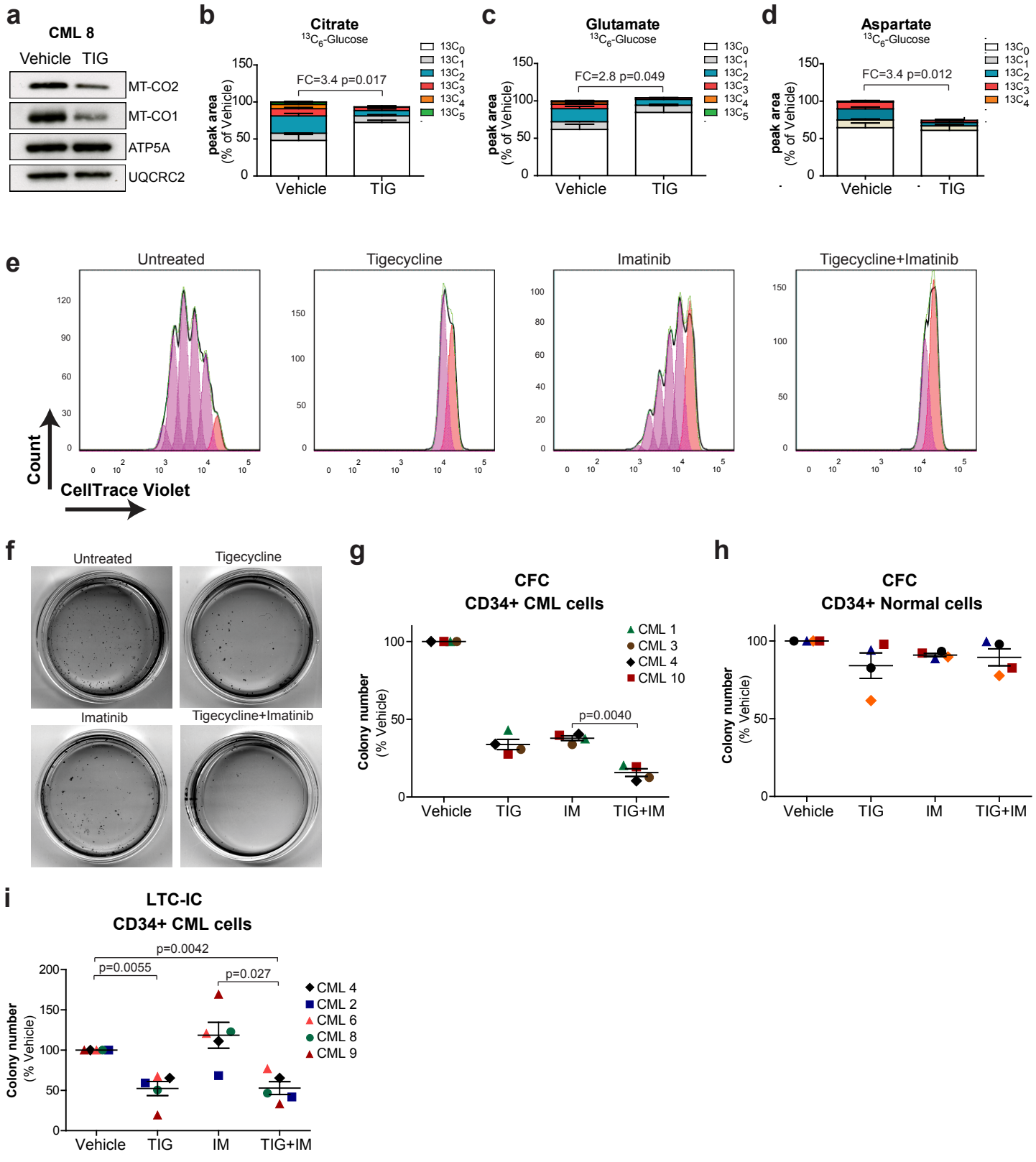
a
CML 8
Vehicle TIG
MT-CO2
MT-CO1
ATP5A
UQCRC2
b
Citrate
13C6-Glucose
FC=3.4 p=0.017
peak area (% of Vehicle)
Vehicle
TIG
c
Glutamate
13C6-Glucose
FC=2.8 p=0.049
d
Aspartate
13C6-Glucose
FC=3.4 p=0.012
13C0
13C1
13C2
13C3
13C4
13C5
e
Untreated
Tigecycline
Imatinib
Tigecycline+Imatinib
Count
CellTrace Violet
f
Untreated
Tigecycline
Imatinib
Tigecycline+Imatinib
g
CFC
CD34+ CML cells
Colony number (% Vehicle)
CML 1
CML 3
CML 4
CML 10
p=0.0040
Vehicle
TIG
IM
TIG+IM
h
CFC
CD34+ Normal cells
i
LTC-IC
CD34+ CML cells
p=0.0042
p=0.0055
p=0.027
CML 4
CML 2
CML 6
CML 8
CML 9

Figure 4

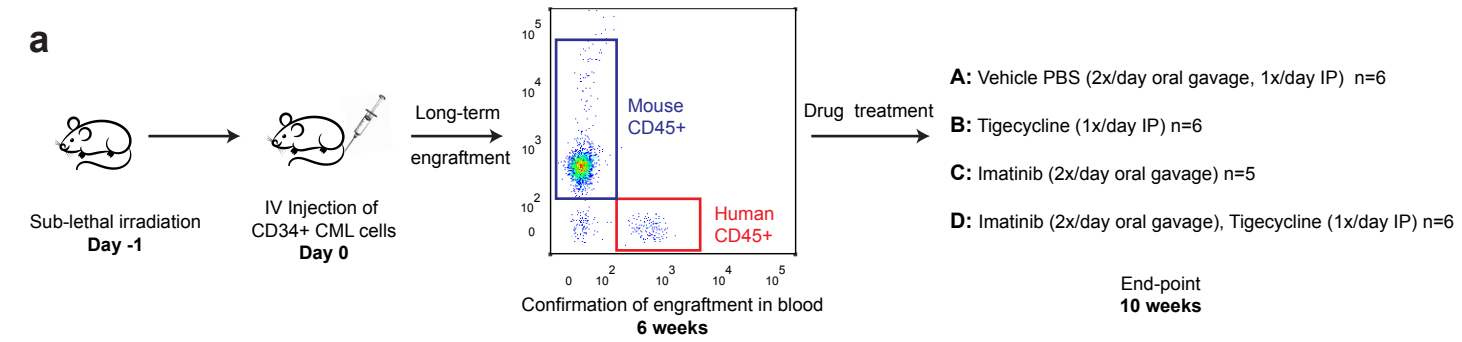
a
Sub-lethal irradiation
Day -1
IV Injection of
CD34+ CML cells
Day 0
Long-term
engraftment
Mouse
CD45+
Human
CD45+
Confirmation of engraftment in blood
6 weeks
Drug treatment
A: Vehicle PBS (2x/day oral gavage, 1x/day IP) n=6
B: Tigecycline (1x/day IP) n=6
C: Imatinib (2x/day oral gavage) n=5
D: Imatinib (2x/day oral gavage), Tigecycline (1x/day IP) n=6
End-point
10 weeks

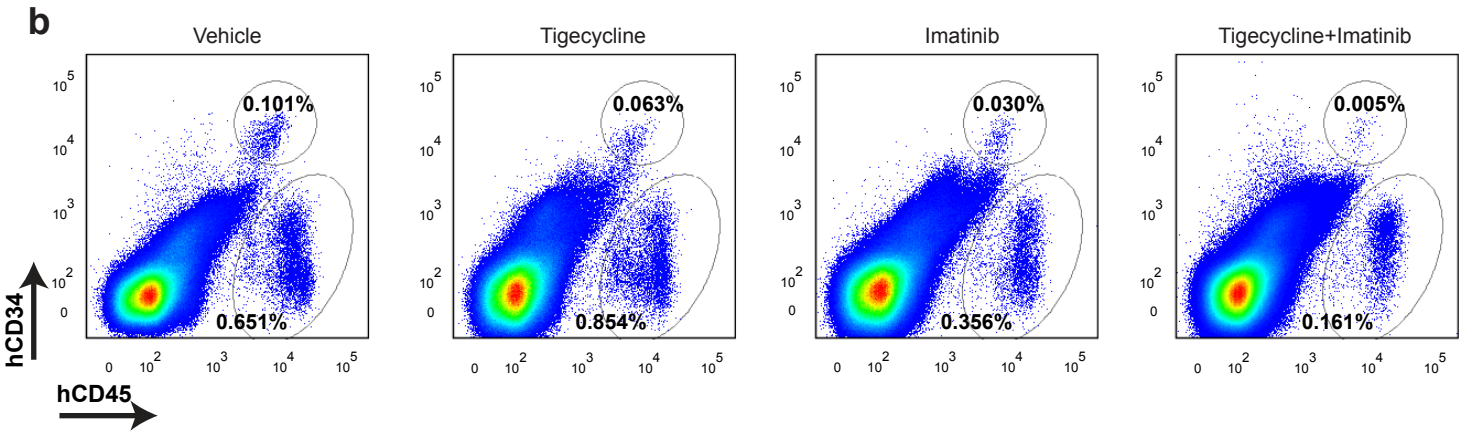
b
Vehicle
Tigecycline
Imatinib
Tigecycline+Imatinib
0.101%
0.651%
0.063%
0.854%
0.030%
0.356%
0.005%
0.161%
hCD34
hCD45

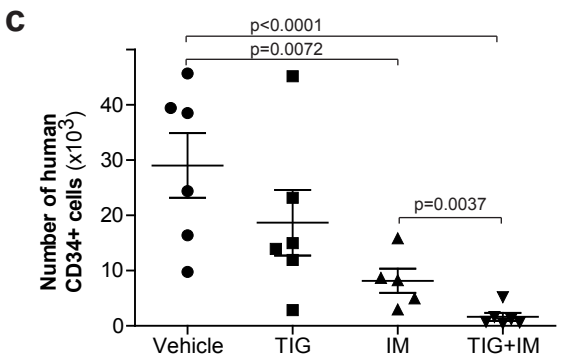
c
p<0.0001
p=0.0072
p=0.0037
Number of human CD34+ cells (x10^3)
Vehicle
TIG
IM
TIG+IM

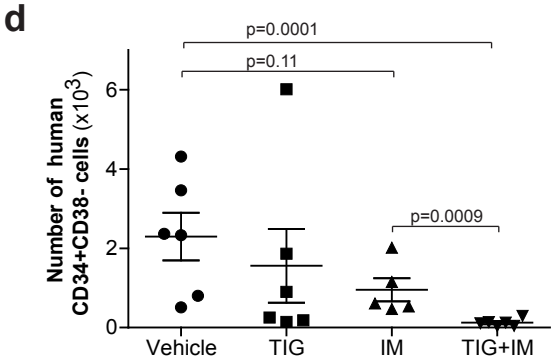
d
p=0.0001
p=0.11
p=0.0009
Number of human CD34+CD38- cells (x10^3)
Vehicle
TIG
IM
TIG+IM

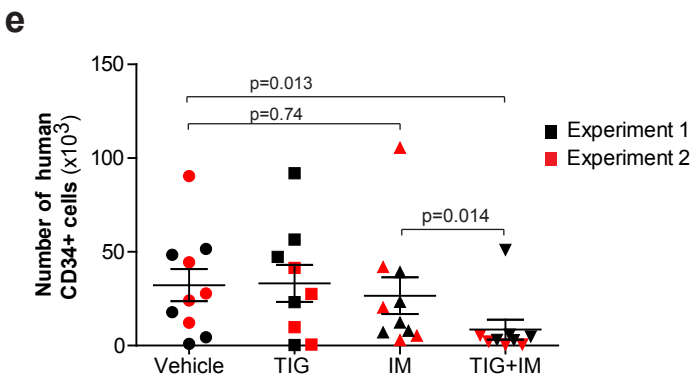
e
p=0.013
p=0.74
p=0.014
Number of human CD34+ cells (x10^3)
Experiment 1
Experiment 2
Vehicle
TIG
IM
TIG+IM

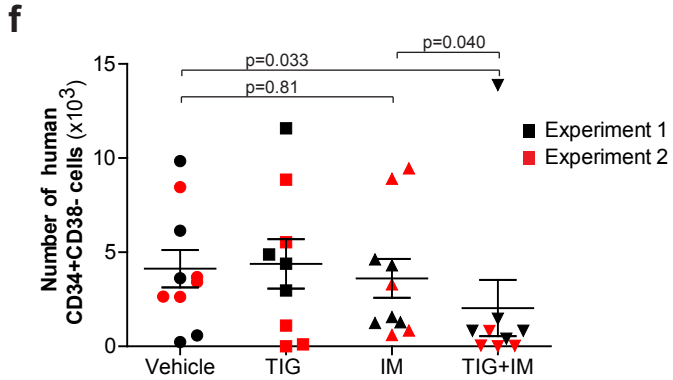
f
p=0.033
p=0.040
p=0.81
Number of human CD34+CD38- cells (x10^3)
Experiment 1
Experiment 2
Vehicle
TIG
IM
TIG+IM